# Investigation of Charge Transfer and Degradation Features in Bilayer Zr-ZrO$_2$

*A.T. Pugachov, V.V. Starikov, A.V. Taranukha, L.M. Udovenko, A.G. Mamalis, and S.N. Lavrynenko*

**The mechanism of charge transfer in bilayer system Zr-ZrO$_2$ and its conductivity in the initial state and after degradation were investigated. The anodization parameter was calculated, permitting to set the thickness of the oxide layer at anodic oxidation of zirconium. The degradation mechanism of layer systems Zr-ZrO$_2$, determined by increasing the oxide conductivity and accompanied by geometrical growth of oxide layer thickness, is outlined in this article.**

## 1. Introduction

At the present time, zirconium and its alloys are applied in nuclear power engineering as construction materials (Ref 1), in chemical engineering because of high corrosion stability (Ref 2) and in medicine (Ref 3). Zirconium is a polymorphic material. The low temperature modification has a hexagonal highly packed grating. Heating up to $T = 1135$ K results transforming it in a body-centered cubic lattice. The temperature of polymorphic transformation of zirconium is increased with dissolution of oxygen (Ref 4).

The characteristic features, of zirconium are determined, in most cases by the availability on its surface of oxide layer with high chemical passivity. Surface oxide will be formed at the contact of metal with oxygen and can increase the thickness, depending on the activity of chemical environment or the influence of other external factors (Ref 5). In interaction with oxygen the formation of metastable oxide phases Zr$_6$O, Zr$_3$O, and ZrO is possible. The most stable oxide of zirconium is ZrO$_2$ (Ref 4). Presence on the metal surface of oxide phases should be taken into account by consideration of electrical and other properties of zirconium because not pure metal but bilayer system metal-oxide in some cases is substantially investigated.

In this article, the charge transfer in the bilayer system Zr-ZrO$_2$ in the initial state and after degradation processes in connecting with an ion exchange between contacting layers is reported. The analysis of such degradation features is presented.

**A.T. Pugachov, V.V. Starikov, A.V. Taranukha, L.M. Udovenko,** and **S.N. Lavrynenko,** National Technical University, "Kharkov Polytechnic Institute", Kharkov, Ukraine; and **A.G. Mamalis,** Project Center for Nanotechnology and Advanced Engineering, NCSR "Demokritos", Athens, Greece. Contact e-mail: mamalis@ims.demokritos.gr.

## 2. Experimental

The samples of zirconium foil were annealed in vacuum $P \sim 10^{-3}$ Pa at temperature $T = 1000$ K for a period $\tau = 1$ h that allowed for mechanical stresses decreasing in the metal and refining its surface. The anodic oxidation technique was employed for the growth of oxide layer on the zirconium surface. As anode zirconium foil and as cathode tantalum foil were used, both metals were placed in an electrolyte (1%—water solution of acetic acid) cell. Note that, the two successive oxidation modes of zirconium are the galvanostatic and voltagestatic. In the galvanostatic mode, the current density was kept constant, $J = 1$ A/m$^2$ at voltage variation in the range from 0 up to 120 V and thickness of the oxide layer $t$ has grown at increased value of anodization voltage, $U_a$ by law:

$$t = \alpha U_a, \tag{Eq 1}$$

where $\alpha$ is the anodization parameter, depending on the nature of the oxidized metal.

In the voltagestatic mode, the voltage on the sample was kept constant and the current at this time decreased at the expense of the oxide chemical composition stoichiometry increase, but oxide thickness in this stage did not change. By decreasing the current by 1-2 orders of magnitude, the process broke off. After anodization the metal-oxide bilayer was flushed in distilled water. The interference color of the surface responded to oxide thickness.

As a result of an anodic oxidation the amorphous oxide layer ZrO$_2$ was formed on the zirconium surface (Fig. 1). The transformation of amorphous oxide layer to the crystalline state was conducted using photon annealing. After such annealing the crystalline oxide phase ZrO$_2$ was monitored on the zirconium surface by x-ray diffraction technique (Fig. 2).

The I-V characteristics of the system Zr-ZrO$_2$-counter electrode were observed. As counter electrode were both the metal pressed electrode with a polished tip in a spherical form and the electrolyte (1%—water solution of acetic acid). In order to compare the results, measurements using both the electrodes were conducted at negative polarity of the base metal, because at positive polarization and use of electrolyte there was a capability of chemical composition and oxide thickness changes. The metal counter electrode allowed for analyzing
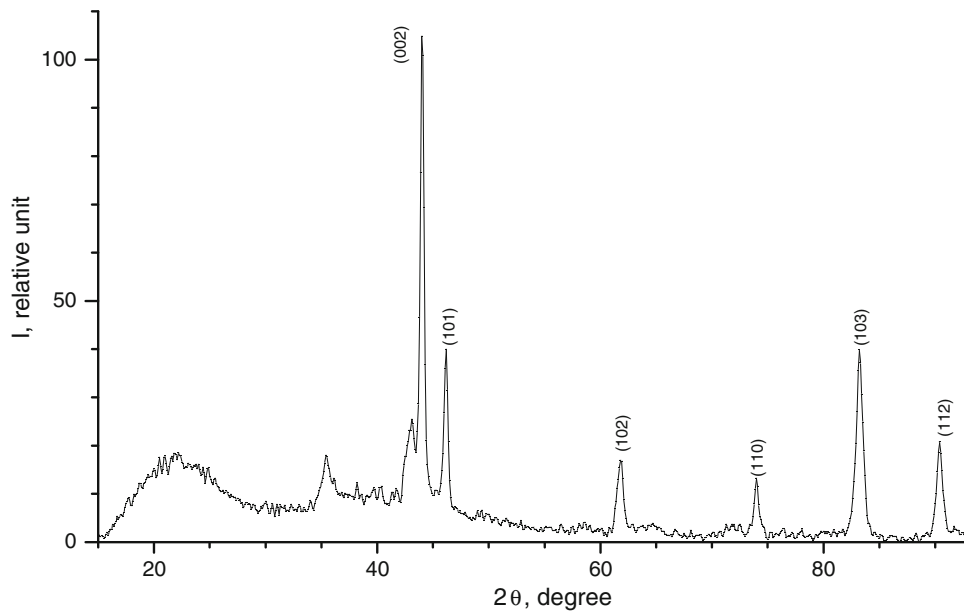
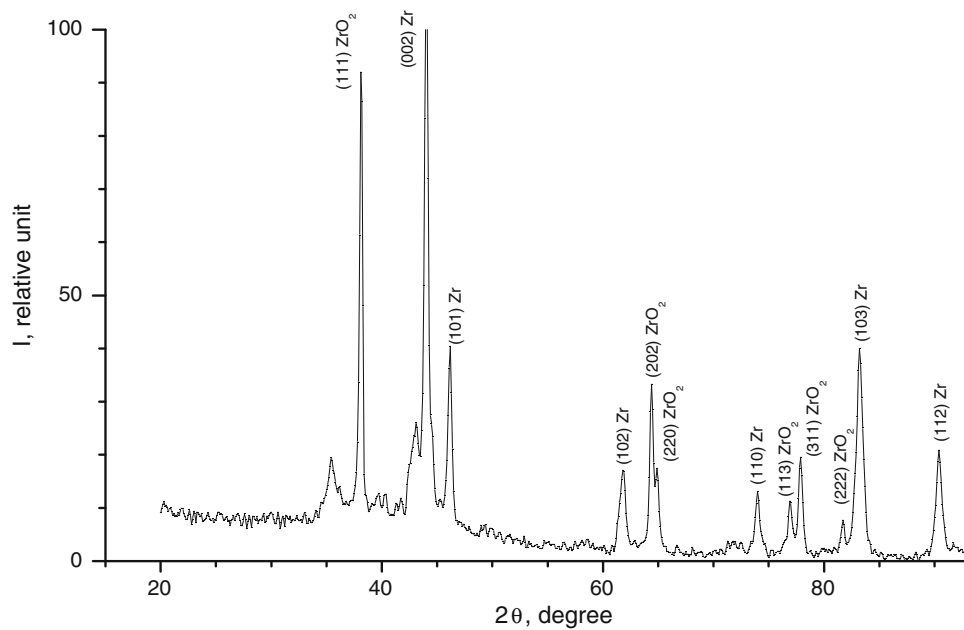**Fig. 1** X-ray pattern of bilayer Zr-ZrO$_2$ in initial state



**Fig. 2** X-ray pattern of bilayer Zr-ZrO$_2$ after photon annealing

the conductivity of the layer system in local segments while the electrolytic contact provided the information about conductivity in the whole surface area of Zr-ZrO$_2$. The experimental results are shown in Fig. 3.

From the I-V characteristics at negative polarity of the base metal both the charge transfer mechanism and the power structure of the forbidden zone of dielectric are identified (Ref 6). Identification of the charge transfer mechanism was provided by the discrimination coefficient, $Q_{ext}$ using characteristic extremums of I-V dependence in bilogarithm scale:

$$\gamma(U) = \frac{d \ln I(U)}{d \ln U} = \frac{U dI(U)}{I(U) dU} \qquad \text{(Eq 2)}$$

For monopolar injection the coefficient, $Q_{ext}$ is calculated in the extremum point $\gamma_{ext}$:

$$Q_{ext} = \frac{(2\gamma_{ext} - 1)^2 |\gamma_{ext} - 1|}{\gamma_{ext}^3} \varepsilon \varepsilon_0 \mu \frac{U_{ext}^2}{j_{ext} t^3}, \qquad \text{(Eq 3)}$$

where $\gamma_{ext}$ is the maximum value of I-V characteristic derivative, $U_{ext}$ is the voltage in the extremum point, and $J_{ext}$ is the current density in the extremum point, respectively.

Differential calculations of the I-V characteristic that was measured in mode of space-charge-limited currents resulted in determining the distribution of electron traps in the forbidden zone of the oxide dielectric (Ref 7).
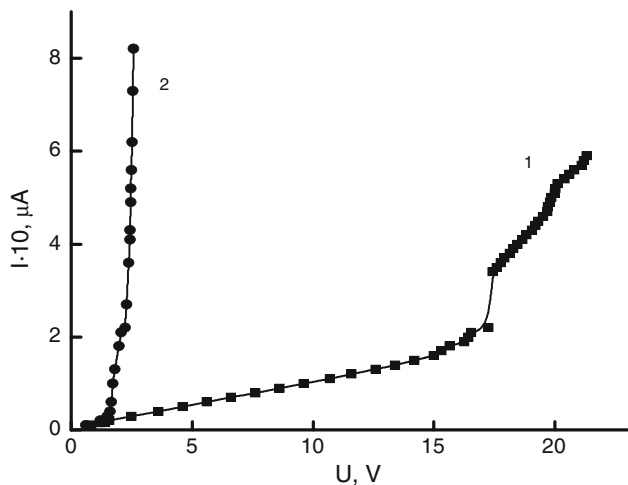
**Fig. 3** I-V characteristics of bilayer systems Zr-ZrO$_2$ with metal pressed electrode (1) and electrolyte counter electrode (2)

The bilayer Zr-ZrO$_2$ in the initial state is a non-equilibrium system, because the Zr-O equilibrium diagram does not contain two-phase equilibrium areas for pure Zr and ZrO$_2$ (Ref 8). The relaxation of bilayers into more thermodynamically stable state occurs through chemical redox reaction at the Zr/ZrO$_2$ interface, during which the oxygen from ZrO$_2$ dissolves in Zr. To investigate the influence of such degradation processes on the electrical conductance of the Zr-ZrO$_2$ the metal-oxide bilayer was annealed in vacuum, e.g., $P \sim 10^{-3}$ Pa at $T = 600$ K during 1, 2, 4, and 8 h.

## 3. Results and Discussion

Information about the anodization parameter, $\alpha_{Zr}$ is necessary for the control of the anodic oxidation process for zirconium. This parameter allows for the determination of the oxide thickness $t$ for the last value of anodization voltage $U_a$, given from Eq 1. Note, however, that the thickness of the oxide layer $t$, at electrochemical oxidation is determined also by Faraday's law as

$$t = \frac{qM\nu}{2SyF\rho}, \qquad \text{(Eq 4)}$$

where $q$ is the charge passed through the galvanic cell during the oxidation process, $M$ is the molecular weight of oxide, $\nu$ is the current efficiency ($\nu = 1$), $S$ is the area of the oxidized surface, $F$ is the Faraday's constant ($9.65 \cdot 10^4$ C/mol), $\rho$ is the oxide density, and $y$ is the parameter depending on the valence of oxygen in the chemical formula of oxide.

Combining Eq (4), (2), and (1) a linear dependence of $U_a$ with time $\tau$ of the anodic oxidation process is obtained as

$$U_a = \frac{IM}{4\alpha_{Zr}SF\rho}\tau, \qquad \text{(Eq 5)}$$

while the anodization parameter for zirconium $\alpha_{Zr}$ is calculated from

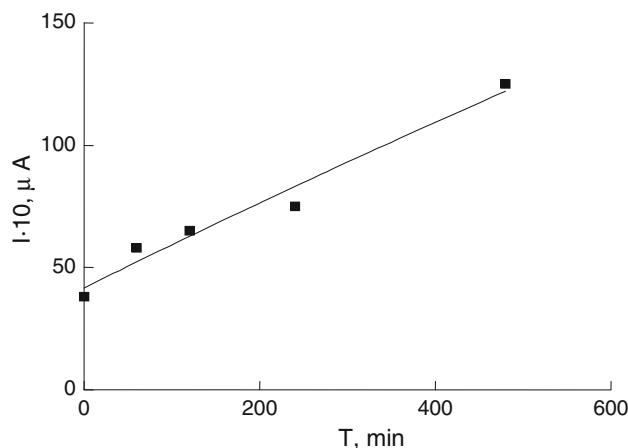$$\alpha_{Zr} = \frac{IM}{4SF\rho\frac{dU_a(\tau)}{d\tau}}, \qquad \text{(Eq 6)}$$



**Fig. 4** Dependence of current from annealing time of bilayers Zr-ZrO$_2$

Using experimental dependence $U_a(\tau)$ on a linear segment the anodization parameter for zirconium has been calculated as $\alpha_{Zr} = 2.1 \cdot 10^{-9}$ m/V.

For the analysis of conductivity in systems Zr-ZrO$_2$-counter electrode the I-V characteristics have been researched. Since the metal counter electrode was the concentrator of electric field the majority of I-V characteristics broke down in the beginning of the measurements. Successfully measured I-V characteristics in broad band of voltage characterized local segments of oxide with minimum quantity of defects. Therefore, the conductivity of such places calculated on an ohmic plot of I-V characteristics, was lower compared with the conductivity calculated for I-V characteristics monitored using electrolyte counter electrode, see Fig. 3. The use of electrolyte counter electrode led to essential growth of the total current.

The form of I-V characteristics was qualitatively identical for both counter electrodes; the ohmic plot with linear dependence of conductivity was replaced by a plot with exponential dependence of current to voltage with an exponent $n \geq 2$.

The numerical differentiation of I-V characteristics has allowed calculating the parameter $\gamma_{ext}$ from Eq 2 and, accordingly, the discrimination coefficient, $Q_{ext}$ from Eq 3 that has enabled to identify the mechanism of charge transfer in the investigated systems. The $Q_{ext}$ values for all the experimental I-V characteristics obtained lie in range from $4.0 \cdot 10^6$ to $1.4 \cdot 10^7$ that significantly exceeds the limiting value $Q_{ext} = 10^3$ constituting the transition regime to currents of monopolar injection. Therefore, in all cases examined the mechanism of charge transfer that changed the ohmic relation was space-charge limited currents. Such information allows to use the original techniques for calculation of an energy spectrum of electron traps in the volume of oxide layer, which specifically determines the conductivity of the bilayer system as a whole (Ref 7).

When annealing the system Zr-ZrO$_2$ the diffusion processes are activated and the stoichiometry of the oxide chemical composition, that connected with the transmission of oxygen from oxide to metal, is violated. Diffusion of oxygen in the system Zr-ZrO$_2$ is a consequence of the absence of interphase equilibrium between ZrO$_2$ and pure zirconium and results in the formation of a transition zone with collected states corresponding to the equilibrium diagram for the pair Zr-O (Ref 8). Such processes affect the conductivity of the system Zr-ZrO$_2$, see Fig. 4. With increased annealing time for the bilayer Zr-ZrO$_2$
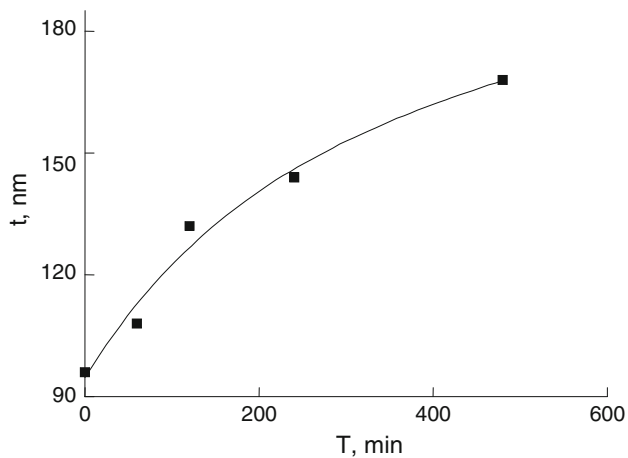
Fig. 5 Dependence of oxide thickness from annealing time of system Zr-ZrO$_2$



Fig. 6 Schemes of oxygen distribution in structures Me-Me$_x$O$_y$, before (1) and after (2) degradation

**Table 1 Diffusivities of oxygen in metals and their oxides (Ref 10)**

| Metal | $D_{metal}$, m$^2$/s | $D_{oxide}$, m$^2$/s |
|---|---|---|
| Ti | $8.32 \cdot 10^{-20}$ | $2.52 \cdot 10^{-30}$ |
| Zr | $1.62 \cdot 10^{-23}$ | $1.20 \cdot 10^{-23}$ |
| Nb | $1.19 \cdot 10^{-16}$ | $4.94 \cdot 10^{-23}$ |
| Ta | $7.23 \cdot 10^{-17}$ | $1.81 \cdot 10^{-22}$ |

prepared on the basis of pure unstrained metal the conductivity increases. The increase of the bilayer conductivity can be explained by applying the same models which are used for bilayers based on other metals of the IV and V groups of the Periodic system, for example, tantalum or niobium. Hence, the increase of conductivity is determined by the increase of oxygen "vacancies" quantity in the bulk of amorphous oxide the stoichiometry of which is violated due to vacuum annealing. Such "vacancies" influence the charge transfer, acting also as "donor" centers, i.e., decreasing the activation energy of the electron transport through the oxide volume (Ref 9).

Among the distinctive features of the degradation process in the system Zr-ZrO$_2$ was the increase of geometrical thickness of the oxide, see Fig. 5. The thickness growth was determined both visually by the interference color of the surface oxide with use of etalon with gradually changing thickness of oxides and by the interference from reflection spectra that were measured for the bilayer Zr-ZrO$_2$ with different oxide thickness.

The diffusion coefficient in metals of IV and V groups of the Periodic system and their oxides is presented in Table 1, taken from Ref 10. Calculations show that the diffusion of oxygen in zirconium is close to that in ZrO$_2$. Therefore, transmission of oxygen through the oxide and the metal layer adjacent to the metal/oxide interface occurred approximately with equal speed, leading to shifting of the interface into the metal regime and to increase the geometrical thickness of ZrO$_2$.

The oxygen distribution in the bilayer system Zr-ZrO$_2$ in comparison with analogous systems based on titanium, niobium, and tantalum before and after degradation is schematically shown in Fig. 6. Such metals as titanium, tantalum,
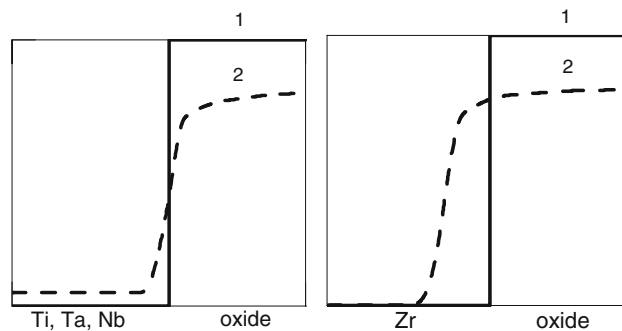
and niobium are unlimited gutters for oxygen which diffuses from oxide. Oxygen concentration in the metals at the expense of higher diffusion rate in comparison with oxygen diffusion in oxide had time to become even in the considerable thickness of metals layer; a link which limits diffusion in the transmission of oxygen in the oxide and through the oxide-metal interface. In this case, the geometrical thickness of the oxide was decreased. Moreover, when the vacuum annealing time was considerably increased, the oxide layer completely disappeared due to the gradual dissolution of oxygen in the base metal.

## 4. Conclusions

Summarizing the main features of the results reported pertaining to the charge and mass transfer in bilayer systems Zr-ZrO$_2$ in the initial stage an after degradation, the following conclusions may be drawn:

- The mechanism of charge transfer at negative polarity of the base metal is determined by space-charge-limited currents.
- From the calculated anodization parameter the thickness of the oxide layer at anodic oxidation of zirconium is obtained, indicating that the zirconium anodic oxide film is inhomogeneous on the surface area that can be determined by structure and impurity in oxidized metal.
- The degradation mechanism of layer systems Zr-ZrO$_2$ is determined by the increase of the oxide conductivity due to violation of its stoichiometry accompanied by geometrical growth of the oxide layer thickness.

## References

1. K. Yueh and B. Cox, Cathodoluminescence Imaging of Oxidised Zirconium Alloys, *J. Nucl. Mater.*, 2004, **323**, p 203–214
2. N. Rajan, C.A. Zorman, M. Mehregany, R. DeAnna, and R. Harvey, Performance of 3C-SiC Thin Films as Protective Coatings for Silicon-Micromachined Atomizers, *Thin Solid Films*, 1998, **315**, p 170
3. X. Liu, A. Huang, C. Ding, and P.K. Chua, Bioactivity, Cytocompatibility of Zirconia (ZrO$_2$) Films Fabricated by Cathodic Arc Deposition, *Biomaterials*, 2006, **27**, p 3904–3911
4. M.E. Drits, *Properties of Elements*, Metallurgy, Moscow, 1985 (in Russian)

5. L.L. Odynets and V.M. Orlov, *Anodic Oxide Films*, Nauka, Leningrad, 1990 (in Russian)

6. A.I. Zuganov and S.V. Sveshnikov, *Injected Phenomena in Semiconductors*, Naukova Dumka, Kyiv, 1981 (in Russian)

7. C. Manfredotti, C. De Blasi, and S. Calassini, Analysis of SCLC Curves by New Direct Method, *Phys. Stat. Solidif. (a)*, 1976, **36**(2), p 569–577

8. I.I. Kornilov and V.V. Glazova, *Interaction of Refractory Metals of Transition Groups with Oxygen*, Nauka, Moscow, 1967 (in Russian)

9. B.T. Boiko et al., Comparison of the Degradation Modes in Sandwich Structures Including Amorphous Oxides of Niobium, Tantalum, *Thin Solid Films*, 1993, **229**, p 207–215

10. G.V. Samsonov, *Physical and Chemical Properties of Oxides*, Metallurgy, Moscow, 1978 (in Russian)